6th International Conference on Multiphase Flow,
ICMF 2007, Leipzig, Germany, July 9 – 13, 2007

Numerical investigation of interfacial mass transfer in bubble train flow within square and rectangular mini-channels

Alexandru Onea[1], Martin Wörner[2] and Dan Gabriel Cacuci[3]

[1,2] Forschungszentrum Karlsruhe, Institute for Reactor Safety, Postfach 3640, 76021 Karlsruhe, Germany
[3] University of Karlsruhe, Institute for Nuclear Technology and Reactor Safety, 76131 Karlsruhe, Germany
E-mail: [1]onea@irs.fzk.de, [2]woerner@irs.fzk.de, [3]cacuci@ikr.uni-karlsruhe.de

Keywords: Bubble train flow, mini-channel, interfacial mass transfer, chemical reaction, direct numerical simulation

Abstract

In the present paper we use the volume-of-fluid method to numerically investigate interfacial mass transfer in bubble train flow within vertical rectangular channels having a hydraulic diameter of 2 mm. Taking advantage of the hydrodynamic axial periodicity of ideal bubble train flow, we restrict our analysis to a single flow unit cell. In our investigations we focus on the influence of the unit cell length (L_{uc} = 2, 2.75 and 3.5 mm), liquid slug length and channel aspect ratio on the mass transfer of an artificial species with low Schmidt number (Sc = 0.8) from the disperse gas into the continuous liquid phase. The mass transfer may be accompanied by a first order homogeneous chemical reaction in the liquid phase or by a first order heterogeneous chemical reaction at the channel walls. The variation of the unit cell length reveals that short unit cells approach the state of concentration equilibrium faster than long unit cells, both for mass transfer without reaction and with homogeneous chemical reaction. In agreement with experimental results (Berčič & Pintar 1997) it is found that the bubble top and bottom contribute to the major part of the interfacial mass transfer. For mass transfer accompanied by a first order heterogeneous chemical reaction the influence of L_{uc} is very small. The variation of the liquid slug length shows that short liquid slugs are more efficient for mass transfer than long liquid slugs in quantitative agreement with experimental data. The investigation of the influence of the channel aspect ratio reveals that square channels are slightly more efficient for pure mass transfer, while large aspect ratio channels are slightly more efficient for mass transfer with species consumption by chemical reaction.

1. Introduction

Within the context of process intensification, significant interest has been focused in the last decade on investigating the flow in miniaturized devices for micro process engineering. For multiphase flow applications e.g. in micro-bubble columns and monolithic reactors, one of the most important advantages as compared to devices of conventional size, is the large interfacial area per unit volume that allows high transfer rates between the phases. For a proper design of such miniaturized reactors, the mass transfer phenomena in two-phase flows have to be investigated in detail. The lack of adequate experimental tools motivates the need to obtain an insight into interfacial mass transfer phenomena by direct numerical simulations.

The numerical investigation of mass transfer can be performed by two different methods. The first approach, which is also employed in this paper, considers the direct solution of the species conservation equation while the flow field, needed for convective mass transfer, is obtained by solving the Navier-Stokes equations in both phases. The advection of the interface is considered by means of an interface "tracking" or "capturing" method. The approach can in principle be applied to any interfacial geometry and to any flow type. However, since the computational time is generally large, the method is restricted to fundamental investigations of scientific interest. The second approach considers the evaluation of mass transfer by means of an empirical mass transfer coefficient for disperse elements of assumed shape and is appropriate for engineering purposes. The model is based on several assumptions, restricting the generality of the approach.

The first numerical simulations of mass transfer coupled with the volume-of-fluid method for interface tracking are reported by Ohta & Suzuki (1996). Their mass transfer study from a drop in a solvent extraction process was restricted to the simple case where the species concentration on both sides of the interface was continuous (i.e. where the distribution coefficient or Henry number H is unity). Refined grids have to be employed for numerical simulations of mass transfer for which the Henry number and/or the Schmidt number (Sc) are large. For large Henry numbers, the evaluation of high mass fluxes across the interface represents the demanding task. For large Schmidt numbers, the convective term plays the dominant role over the diffusion term, leading to a thin concentration boundary layer.

Petera & Weatherley (2001) numerically investigate the mass transfer from a falling axisymmetric drop using a finite element approach. They report good agreement between the numerical solution and experimental data for the extraction of ethanol from an ethanol-water mixture into a n-decanol solution. The internal recirculation within the drop, the development of the recirculation zone in the

continuous phase and the increased surface area are the factors that control the mass transfer. The developed concentration wake is smooth, symmetrical and regular, characteristics reported also by Bothe et al. (2004), Koynov et al. (2005) and Onea (2006) for bubble Reynolds number ranging between 1 and 30. Bothe et al. (2003) report numerical simulations of the mass transfer of oxygen from single bubbles and bubble chains rising in aqueous solution with large values of the Schmidt number (*Sc* up to 1000).

While the investigations mentioned above concern the mass transfer from spherical or ellipsoidal bubbles or drops, bubbles in millimeter or sub-millimeter channels are often elongated and the corresponding flow regime is known as Taylor flow or bubble train flow. Numerical investigations of the mass transfer in Taylor flow within narrow circular channels are reported by Irandoust & Andersson (1989), Kreutzer et al. (2001) and van Baten & Krishna (2004). In these papers a volumetric mass transfer coefficient is developed based on the separate contribution of the hemispherical caps and lateral sides of the bubbles. In all models the volumetric mass transfer coefficient depends on the channel diameter. It is reported that the major contribution to the mass transfer is realized through the lateral sides of the gas bubble. Berčič & Pintar (1997) have reported an empirical correlation for the volumetric mass transfer coefficient being independent of the channel diameter. Also, in the latter study, it is reported that the major part of the interfacial mass transfer occurs through the surfaces exposed to the liquid slug (since the liquid film is saturated). Therefore, the length of the liquid slug is found to have a significant influence on mass transfer. Vandu et al. (2005) conclude in their study that the occurrence of the saturation in the liquid film in the experiments of Berčič & Pintar (1997) decreases the efficiency of the liquid film for mass transfer, while the liquid film is not saturated in the study performed by van Baten & Krishna (2004). A criterion that quantifies the degree of liquid film saturation is proposed within the present study.

When deriving the mass transfer coefficient in two-phase flows, a controversial aspect is the choice of the appropriate concentration difference. Paschedag et al. (2005) and Yang & Mao (2005) proposed a mass transfer coefficient based on the concentration in the bulk phase far away from the interface and the mean concentration in the disperse phase. A formulation based on the concentration at the interface has been reported by Paschedag et al. (2002). For mass transfer in confined mini-systems, defining the concentration in the bulk phase far away from the bubble as well as at the interface is difficult. Therefore, a new formulation is proposed and discussed within this paper.

The outline of the present paper is as follows. In section 2 we present the governing equations, describe the numerical method and perform a validation of the species conservation equation by test problems. In section 3 we present the results of numerical simulations for the mass transfer in bubble train flow in square and rectangular mini-channels. The conclusions are given in section 4.

Nomenclature

A_i	bubble interfacial area (m^2)
a_i	local volumetric interfacial area concentration made non-dimensional by L_{ref} (-)
c	concentration (mol m^{-3})
Ca	Capillary number (-)
d	diameter (m)
D	diffusion coefficient (m^2 s^{-1})
Da	Damköhler number (-)
$Eö$	Eötvös number (-)
Eu	Euler number (-)
f	liquid volumetric fraction (-)
Fo	Fourier number (-)
g	gravitational constant (m^2 s^{-1})
H	Henry number (-)
i,j,k	mesh cell index (-)
$\mathbf{j}$	molar flux (mol m^{-2} s^{-1})
J	total superficial velocity (m s^{-1})
k_{hmg}	constant of homogeneous reaction (s^{-1})
k_{htg}	constant of heterogeneous reaction (m^{-1} s^{-1})
k_L	mass transfer coefficient (m s^{-1})
L	length (m)
$\hat{\mathbf{n}}_i$	unit normal vector to the interface pointing into the liquid (-)
Mo	Morton number (-)
p	pressure (N m^{-2})
r	non-dimensional sink term for homogeneous chemical reaction (-)
Re	Reynolds number (-)
Sc	Schmidt number (-)
t	time (s)
Δt	time step width (s)
U	velocity (m s^{-1})
$\mathbf{v}$	velocity field (m s^{-1})
V	volume (m^3)
We	Weber number (-)
x,y,z	Cartesian coordinates (m)
Z	dimensionless relative velocity (-)

Greek letters

ε	gas volume fraction (-)
μ	dynamic viscosity (Pa s)
ρ	density (kg m^{-3})
κ	interface curvature made non-dimensional by L_{ref} (-)
σ	surface tension (N m^{-1})
θ	non-dimensional time (-)

Subscripts and superscripts

0	initial state
B	bubble
eq	equilibrium
exp	exposure
G	gas
h	hydraulic
hmg	homogeneous
htg	heterogeneous
i	interface
L	liquid
LF	liquid film
LS	liquid slug
m	mixture quantity
ref	reference
uc	unit cell

2. Numerical method

2.1 Hydrodynamic equations

The conservation equations for mass and momentum describing the flow of two immiscible incompressible fluids with constant material properties (density, viscosity, surface tension) can be written in the following non-dimensional formulation:

$$\nabla \cdot \mathbf{v}_\mathrm{m} = 0 \tag{1}$$

$$\frac{\partial f}{\partial t} + \nabla \cdot f\,\mathbf{v}_\mathrm{m} = 0 \tag{2}$$

$$\begin{aligned}\frac{\partial(\rho_\mathrm{m}\mathbf{v}_\mathrm{m})}{\partial\theta} + \nabla\cdot\rho_\mathrm{m}\mathbf{v}_\mathrm{m}\mathbf{v}_\mathrm{m} &= -\nabla P + \frac{a_\mathrm{i}\kappa\hat{\mathbf{n}}_\mathrm{i}}{We_\mathrm{ref}} \\ &+ \frac{1}{Re_\mathrm{ref}}\nabla\cdot\mu_\mathrm{m}\left(\nabla\mathbf{v}_\mathrm{m} + (\nabla\mathbf{v}_\mathrm{m})^\mathrm{T}\right) \\ &- (1-f)\frac{E\ddot{o}_\mathrm{ref}}{We_\mathrm{ref}}\hat{\mathbf{e}}_\mathrm{g} + Fr_\mathrm{ref}\hat{\mathbf{e}}_\mathrm{g} + \frac{L_\mathrm{ref}}{L_\mathrm{axial}}Eu_\mathrm{ref}\hat{\mathbf{e}}_\mathrm{axial}\end{aligned} \tag{3}$$

In the above equations, ρ_m is the mixture density

$$\rho_\mathrm{m} \equiv \frac{f\rho_\mathrm{L} + (1-f)\rho_\mathrm{G}}{\rho_\mathrm{L}}, \tag{4}$$

μ_m is the mixture viscosity

$$\mu_\mathrm{m} \equiv \frac{f\mu_\mathrm{L} + (1-f)\mu_\mathrm{G}}{\mu_\mathrm{L}}, \tag{5}$$

$\mathbf{v}_\mathrm{m}$ is the centre-of-mass velocity

$$\mathbf{v}_\mathrm{m} \equiv \frac{1}{U_\mathrm{ref}}\frac{f\rho_\mathrm{L}\mathbf{v}_\mathrm{L} + (1-f)\rho_\mathrm{G}\mathbf{v}_\mathrm{G}}{f\rho_\mathrm{L} + (1-f)\rho_\mathrm{G}} \tag{6}$$

and f is the local liquid volumetric fraction (which is 1 for liquid filled cells, 0 for gas filled cells and which may take any value between 0 and 1 for interface cells). The non-dimensional time θ is given by:

$$\theta \equiv \frac{t}{t_\mathrm{ref}} = t\frac{U_\mathrm{ref}}{L_\mathrm{ref}}, \tag{7}$$

where L_ref is a reference length scale and U_ref is a reference velocity scale.

Since the single-field Navier-Stokes equation (3) shall be applicable to a domain with periodic boundary conditions, the dimensionless "reduced" pressure P has been introduced, which is related to the dimensional physical pressure p via:

$$P \equiv \frac{1}{\rho_\mathrm{L}U_\mathrm{ref}^2}\left(p + \frac{\overline{p}_0 - \overline{p}_{L_\mathrm{axial}}}{L_\mathrm{axial}}\hat{\mathbf{e}}_\mathrm{axial}\cdot\mathbf{x}\right) \tag{8}$$

Here, $\overline{p}_0$ is the plane-average of p over the cross section at $\mathbf{x} = 0$ while $\overline{p}_{L_\mathrm{axial}}$ is the plane-average across the cross section at $\mathbf{x} = L_\mathrm{axial}\hat{\mathbf{e}}_\mathrm{axial}$ and $\hat{\mathbf{e}}_\mathrm{axial}$ is the unit vector in axial direction. Due to the decomposition of the pressure term according to Eq. (8) the buoyancy term appears in the Navier-Stokes equation with $\hat{\mathbf{e}}_\mathrm{g}$ as the unit vector in the direction of gravity.

The definitions of the dimensionless numbers in Eq. (3) based on the reference scales are:

$$Re_\mathrm{ref} \equiv \frac{\rho_\mathrm{L}L_\mathrm{ref}U_\mathrm{ref}}{\mu_\mathrm{L}},\ E\ddot{o}_\mathrm{ref} \equiv \frac{(\rho_\mathrm{L}-\rho_\mathrm{G})gL_\mathrm{ref}^2}{\sigma} \tag{9}$$

$$We_\mathrm{ref} \equiv \frac{\rho_\mathrm{L}L_\mathrm{ref}U_\mathrm{ref}^2}{\sigma},\ Eu_\mathrm{ref} \equiv \frac{\overline{p}_0 - \overline{p}_{L_\mathrm{axial}}}{\rho_\mathrm{L}U_\mathrm{ref}^2},\ Fr_\mathrm{ref} \equiv \frac{gL_\mathrm{ref}}{U_\mathrm{ref}^2} \tag{10}$$

The above equations have been implemented in our in-house computer code TURBIT-VOF (Sabisch et al. 2001, Ghidersa et al. 2004) which is based on a finite volume method and employs a regular Cartesian staggered grid. The strategy for solution of Eqs. (1) and (3) involves a projection method where the resulting Poisson equation is solved by a conjugate gradient method. For time integration of the momentum equation (3) an explicit third-order Runge-Kutta scheme is employed. All spatial derivatives are approximated by second order central difference schemes.

The volume fraction advection equation (2) is solved by means of a volume-of-fluid method with interface reconstruction. The interface is locally approximated as a plane whose orientation and location within a mesh cell are determined by the EPIRA algorithm (Exact Plane Interface Reconstruction Algorithm, Sabisch et al. 2001). In the un-split advection step of the VOF procedure the fluxes of liquid over the cell faces are computed in a geometrical manner.

2.2 Species conservation equation for mass transfer

To allow for simulation of mass transfer phenomena with TURBIT-VOF, the non-dimensional species conservation equation

$$\frac{\partial c_\mathrm{m}}{\partial\theta} + \nabla\cdot(c_\mathrm{m}\mathbf{v}_\mathrm{m}) = -\frac{1}{Re_\mathrm{ref}Sc_\mathrm{ref}}\nabla\cdot\mathbf{j}_\mathrm{m} + r \tag{11}$$

has been implemented in the code and can be solved for an arbitrary number of chemical species (Onea, 2006). The definition of the non-dimensional mixture concentration

$$c_\mathrm{m} \equiv \frac{fc_\mathrm{L} + (1-f)Hc_\mathrm{G}}{c_\mathrm{ref}} \tag{12}$$

involves the Henry number (or Henry coefficient) which expresses the ratio between the equilibrium concentrations on both sides of the interface:

$$H \equiv \frac{c_\mathrm{L}^\mathrm{eq}}{c_\mathrm{G}^\mathrm{eq}} \tag{13}$$

Further quantities appearing in Eq. (11) are the dimensionless sink term due to an optional first order homogeneous chemical reaction in the liquid phase $r = k_\mathrm{hmg}t_\mathrm{ref}c_\mathrm{L}/c_\mathrm{ref}$, and the reference Schmidt number

$$Sc_\mathrm{ref} \equiv \frac{\mu_\mathrm{L}}{\rho_\mathrm{L}D_\mathrm{ref}} \tag{14}$$

where D_ref is a reference diffusivity which is here the diffusivity of the species in the liquid phase D_L so that $Sc_\mathrm{ref} = Sc_\mathrm{L}$. Alternative to a first order homogeneous chemical reaction, a first order heterogeneous chemical reaction at the channel walls may be considered, which is implemented by means of the wall boundary conditions

for Eq. (11). In the current implementation, the species conservation equation is without feedback on the Navier-Stokes equations, i.e. the mass transfer affects neither the velocity field nor the bubble size and shape.

In our approach we assume that at the interface the concentrations are always in equilibrium. Then, the inclusion of the Henry number H on the right hand side of definition (12) ensures that c_m is always continuous across the interface. By this procedure we avoid possible numerical difficulties which might appear when dealing with the physical concentrations c_G and c_L which are discontinuous at the interface for $H \neq 1$. Such a transformation has recently become popular for interface mass transfer studies (Petera & Weatherley 2001, Bothe et al. 2003 and Yang & Mao 2005). Thus, while in the liquid c_m corresponds to c_L/c_{ref}, in the gas phase it corresponds to Hc_G/c_{ref}. A significant drawback of this transformation is, however, that the continuity of diffusive mass flux across the interface

$$\left[\mathbf{j}\cdot\hat{\mathbf{n}}_i\right] = (\mathbf{j}_L - \mathbf{j}_G)\cdot\hat{\mathbf{n}}_i = (-D_L\nabla c_L + D_G\nabla c_G)\cdot\hat{\mathbf{n}}_i = 0 \qquad (15)$$

is not fulfilled by Eq. (11) when the diffusive mixture molar flux $\mathbf{j}_m$ is – in accordance to Fick's first law – formulated in terms of the gradient of c_m as

$$\mathbf{j}_m = -D_m\nabla c_m \qquad (16)$$

Instead, there is a jump in the derivative of the mass flux in normal direction which only vanishes for $H = 1$. The problem to fulfill condition (15) not only for $H = 1$ but for the general case $H \neq 1$ can be solved by computing the mixture diffusivity D_m and the diffusive flux close to the interface in an appropriate manner.

2.3 Computation of diffusive interfacial mass flux

We illustrate the computation of the interfacial diffusive flux for the x-direction. For a mesh cell (i,j,k) the cell centred mixture diffusivity is computed from the discrete value of the volume fraction:

$$D_{m;i,j,k} = \frac{f_{i,j,k}D_L + (1-f_{i,j,k})D_G}{D_{ref}} \qquad (17)$$

However, since the diffusive term is discretized with a central difference scheme, the diffusivity D_m is needed at the position of the cell face i+1/2. For neighboring mesh cells i and i+1 which contain only one phase, the cell face diffusivity simply corresponds to the diffusivity of that phase. For neighboring mesh cells that contain different phases, the formulations proposed by Patankar (1980) and Davidson & Rudman (2002) for computation of the cell face diffusivity have been modified and implemented in TURBIT-VOF. The modifications are based on an appropriate inclusion of the Henry number H and are necessary since the original formulations are based on the assumptions that the concentration field is continuous at interface and that the interfacial diffusive fluxes are equal. The formulation of Patankar (1980) considers the situation where the interface coincides with the common face of two neighboring cells. The original and extended formulations valid for an uniform grid are presented in Table 1 while the conditions for allocating the cell Henry number as $H_{i,j,k} = H$ are listed in Table 2. For other cases not listed in Table 2 we set $H_{i,j,k} = 1$. Similar modifications apply to the computation of the interfacial diffusive flux, see Onea (2006) for details.

Table 1: Computation of mixture diffusivity at face i+1/2.

Author	Cell face diffusivity
Patankar (1980)	$D_{m;i+1/2,j,k} = \dfrac{2D_{m;i,j,k}D_{m;i+1,j,k}}{D_{m;i,j,k} + D_{m;i+1,j,k}}$
This study	$D_{m;i+1/2,j,k} = \dfrac{2D_{m;i,j,k}D_{m;i+1,j,k}}{H_{i,j,k}D_{m;i,j,k} + D_{m;i+1,j,k}}$
Davidson & Rudman (2002)	$D_{m;i+1/2,j,k} = \dfrac{D_{m;i,j,k}D_{m;i+1,j,k}}{D_{m;i,j,k}(1.5-\lambda_i) + D_{m;i+1,j,k}(\lambda_i - 0.5)}$ $\lambda_i = \mathrm{Max}\left(\mathrm{Min}\left(f_{i,j,k} + f_{i+1,j,k}, 1.5\right), 0.5\right)$
This study	$D_{m;i+1/2,j,k} = \dfrac{D_{m;i,j,k}D_{m;i+1,j,k}}{H_{i,j,k}D_{m;i,j,k}(1.5-\lambda_i) + D_{m;i+1,j,k}(\lambda_i - 0.5)}$

Table 2: Conditions for setting the cell Henry number as $H_{i,j,k} = H$.

$f_{i,j,k}$	$f_{i+1,j,k}$
$0 < f_{i,j,k} < 1$	0
0	$0 < f_{i+1,j,k} < 1$
1	0
0	1

2.4 Validation of the species conservation equation

The implementation of the species conservation equation in TURBIT-VOF is validated against theoretical solutions of a number of different mass transfer problems, see Onea (2006). The validation for the diffusive term has been done by comparison to the one-dimensional time-dependent analytical solution of Crank (1994). Two stagnant fluids separated by a plane interface are considered. The initial dimensionless concentration in the liquid is zero, while in the gas phase it is unity. Figure 1 displays a comparison between analytical and numerical solutions for $H = 0.5$ and 5 for a diffusivity ratio $D_G/D_L = 10$. No significant differences between the two modified formulations for the mixture diffusivity according to Table 1 have been found (Onea 2006). In the following simulations the modified formulation of Davidson & Rudman (2002) has been employed. Comparisons for further values of H and D_G/D_L can be found in Onea (2006). In general, very good agreement between numerical and analytical solution is always obtained for $H < 1$. When the Henry number is much larger than unity, very sharp concentration gradients exist at the interface so that a good agreement between numerical and analytical solution is only obtained when this gradient is adequately resolved by a sufficiently fine grid. To test the implementation of the diffusion term for multi-dimensional problems, similar tests have been performed for the mass transfer through a cylindrical interface, see Onea (2006).

The convective term and the sink term have been validated against theoretical solutions of Apelblat (1980) for steady-state mass transfer with and without species consumption by a first order homogeneous or heterogeneous chemical reaction in two-dimensional single phase flow over a horizontal wall. The fluid is flowing in horizontal direction with a constant uniform velocity. The initial concentration in the domain is zero.

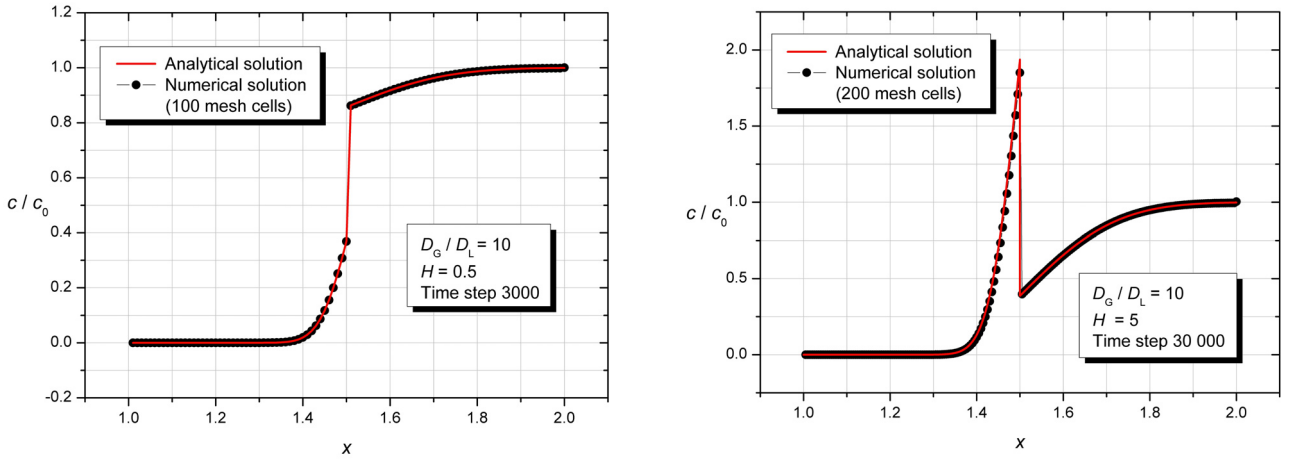

Figure 1: Comparison between numerical solution (black dots) and analytical solution (solid red line) for one-dimensional mass transfer through a plane interface at x = 1.5 for Henry number H = 0.5 (left figure) and H = 5 (right figure) for D_G/D_L = 10 at a certain instant in time.

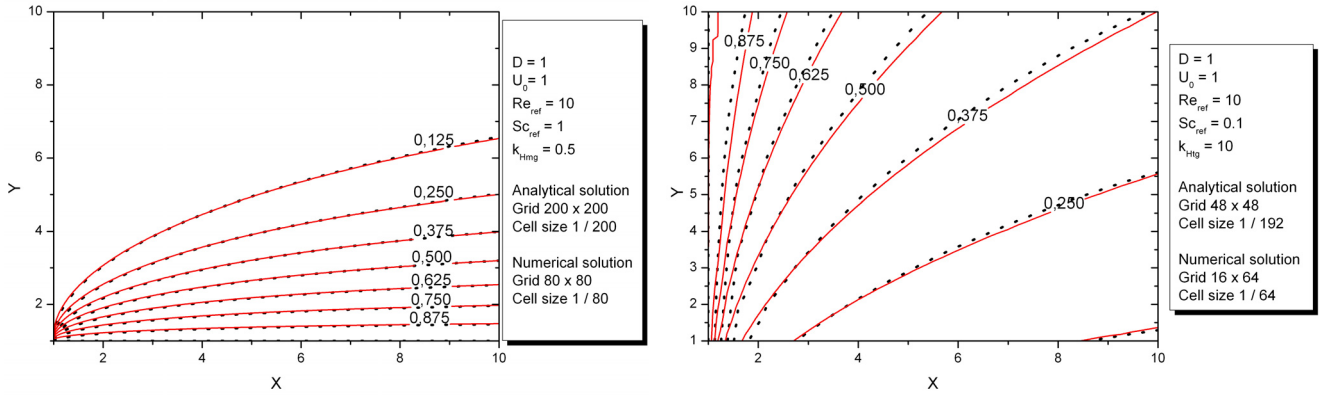

Figure 2: Comparison between theoretical solution (solid red lines) and numerical solution (dotted black lines) for two-dimensional mass transfer with species consumption by first order homogeneous reaction (left figure) and heterogeneous reaction (right figure).

In the first case the species is consumed by a first order homogeneous reaction in the entire domain and the wall is held at constant dimensionless concentration c = 1. In the second case the species is consumed by a first order heterogeneous reaction at the wall and the inlet and the upper boundary of the domain are held at constant concentration c = 1. For all cases investigated good agreement has been found between the theoretical and the numerical solutions obtained with TURBIT-VOF, as displayed in Figure 2 (see also Onea, 2006).

3. Mass transfer in bubble train flow

3.1 Numerical set-up and parameters

Flows in narrow devices often exhibit some regularity, i.e. internal flow structures repeat themselves. For developed two-phase flows exhibiting periodicity in axial direction a unit cell represents that part of the flow that continuously repeats. From the numerical point of view this feature is often exploited by reducing the computational domain from the system size to the much smaller size of a unit cell. In our simulations, the unit cell consists of one bubble and one liquid slug, as displayed in Figure 3. The coordinate system is defined so that the y-axis represents the stream-wise vertical direction with the gravity vector pointing in negative y-direction, while the x- and z-axis represent the wall-normal directions. Periodic boundary conditions are employed at the top and bottom of the unit cell. The computational domain is a rectangular parallelepiped with size $L_x \times L_{uc} \times L_y$. We consider the co-current vertical bubble train flow within square and rectangular vertical channels having the hydraulic diameter of d_h = 2mm. In all simulations the value of the reference velocity is U_{ref} = 0.0264 m/s and $\hat{\mathbf{e}}_{axial} = -\hat{\mathbf{e}}_g = \hat{\mathbf{e}}_y$.

The simulations are started without mass transfer from a situation where an axi-symmetric elongated bubble (similar to the one in Figure 3) is placed in the centre of the domain and where both gas and liquid are initially at rest. The flow is driven by buoyancy and by the external pressure difference. After a short transient phase, the bubble adopts a steady shape and rises with constant velocity.

The pressure difference $\overline{p}_0 - \overline{p}_{L_{axial}}$ respectively the Euler number Eu_{ref} is adjusted in such a manner so that almost the same bubble velocity U_B is obtained for all simulations that shall be compared. This is to ensure that the capillary number

$$Ca \equiv \frac{\mu_L U_B}{\sigma} \tag{18}$$

and the bubble Reynolds number

$$Re_B \equiv \frac{\rho_L d_h U_B}{\mu_L} \tag{19}$$

are the same for these cases.

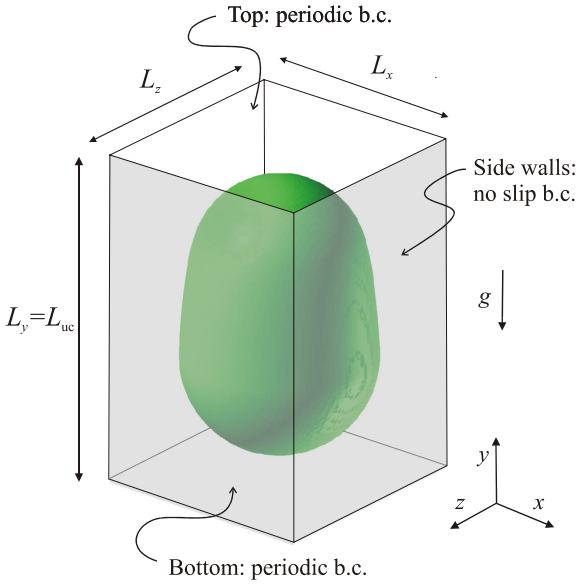

Figure 3: Sketch of computational domain and coordinate system.

The physical properties of the fluids are given in Table 3. The fluids considered are silicone oil as the continuous liquid phase and "air" as the dispersed phase. However, the "air" density and viscosity are set 10 times higher than for real air, in order to by-pass the increased CPU time of the Poisson solver for the real density ratio. As shown in Wörner et al. (2007), this artificial increase of ρ_G and μ_G does not affect the velocity and the bubble shape. The fluid properties presented in Table 3 result in the following Morton number:

$$Mo \equiv \frac{g(\rho_L - \rho_G)\mu_L^4}{\rho_L^2 \sigma^3} = 49.26 \times 10^{-4} \tag{20}$$

When a fully developed flow has been reached, the simulation of mass transfer is launched. In the gas phase, the initial concentration is set to $c_G = c_{ref} = 1$ mol/m^3 which corresponds to the dimensionless concentration $c_m = H$ within the bubble. The initial concentration in the continuous liquid phase is set to zero.

The diffusivities of the species in both phases are given in Table 3. The gas diffusivity corresponds to the diffusivity of oxygen in air, while the diffusivity in the liquid has been deliberately chosen approximately 1000 times higher than the diffusivity of oxygen in water. Therefore, in all the present simulations the Schmidt number for the liquid phase Sc_L is about 0.8. For such a Schmidt number of order unity the thickness of the concentration boundary layer is about the same as that of the viscous boundary layer. Thus, there is no need from mass transfer aspects to use a finer grid than is already required from pure hydrodynamic aspects. Hasegawa & Kasagi (2006) discuss the grid requirements for turbulent mass transfer at a flat free surface. They estimate that the number of grid points is proportional to $Sc^{3/2}$. Thus, realistic Schmidt numbers of order 1000 require grids that are much finer than can be afforded here. Beside the grid requirement aspect for high Schmidt number flows, there is also a second aspect for the artificial increase of the species diffusivity in the liquid phase. Due to the increase of D_L, diffusive processes in the liquid phase are much faster and the simulation time can be drastically reduced.

Table 3: Physical properties of the phases.

Fluid properties	Liquid	Gas
Density (kg m^{-3})	957	11.7
Dynamic viscosity (Pa s)	0.048	1.824×10^{-4}
Species diffusivity (m^2 s^{-1})	62.24×10^{-6}	19.16×10^{-6}
Surface tension (N m^{-1})	0.02218	

3.2 Influence of the unit cell length on mass transfer

In our first series of simulations we consider a square channel with $L_x = L_z = L_{ref} = 2$ mm. To investigate the influence of the length of the unit cell on mass transfer, three values of L_{uc} are considered, namely $L_{uc} = 2$ mm, 2.75 mm and 3.5 mm. In all cases the gas content within the computational domain is $\varepsilon = 33\%$. The parameters for the simulations performed are displayed in Table 4. For all these cases the value of Ca is about 0.208 and that of Re_B is about 3.84. For the influence of the unit cell length on the hydrodynamics of bubble train flow we refer to Wörner et al. (2004, 2007). In the latter paper also a grid refinement study is performed which shows that a uniform grid with 48 × 48 mesh cells per channel cross-section is sufficiently fine. The time step width used for all three cases is $\Delta t / t_{ref} = 2.5 \times 10^{-5}$.

Table 4: Parameters for the study of the influence of the unit cell length on mass transfer.

Case	A	B	C
L_{uc} (mm)	2	2.75	3.5
Grid	48×48×48	48×66×48	48×84×48
Eu_{ref} - Fr_{ref} (-)	27.03	26.23	23.8
U_B (m s^{-1})	0.0964	0.0964	0.0969
U_L (m s^{-1})	0.0319	0.0345	0.0349
A_i/V_{uc} (m^{-1})	1168.8	1476.5	1770.7
d_B/d_h (-)	0.822	0.846	0.858
U_B/J (-)	1.812	1.755	1.749
Z (-)	0.448	0.43	0.428

Figure 4 shows the computed steady bubble shape in a vertical mid-plane for all cases. Since in all cases the gas hold-up is fixed to 33%, an increase of L_{uc} does not only result in an increase of the length of the bubble but also of the liquid slug. Also shown in Figure 4 is the non-dimensional velocity field in a frame of reference moving with the bubble. One can observe a toroidal vortex in the bubble and – for case B and C – one in the liquid slug. Though the bubble velocity is similar in all cases, one can observe that the intensity of the toroidal vortex in the bubble is proportional to the length of the unit cell. Also the liquid velocity is proportional to L_{uc}, meaning that long unit cells exhibit more intense recirculation within the liquid slug than short liquid slugs.

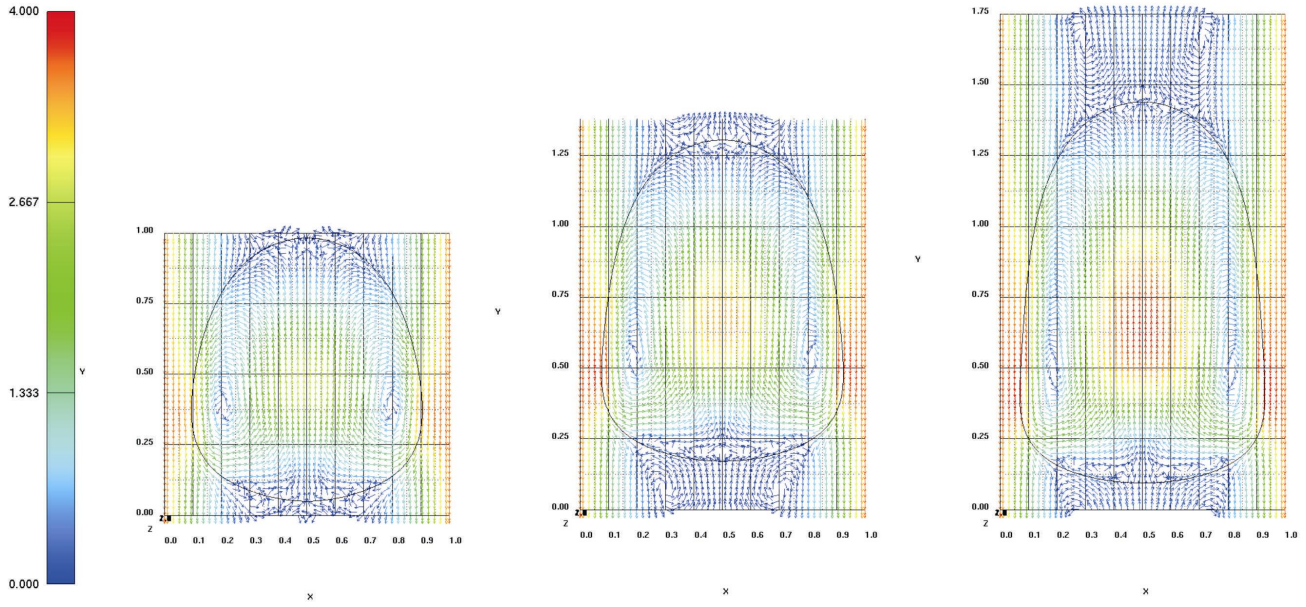

Figure 4: Velocity field in moving frame of reference at z = 1 mm for case A (left), case B (middle) and case C (right).

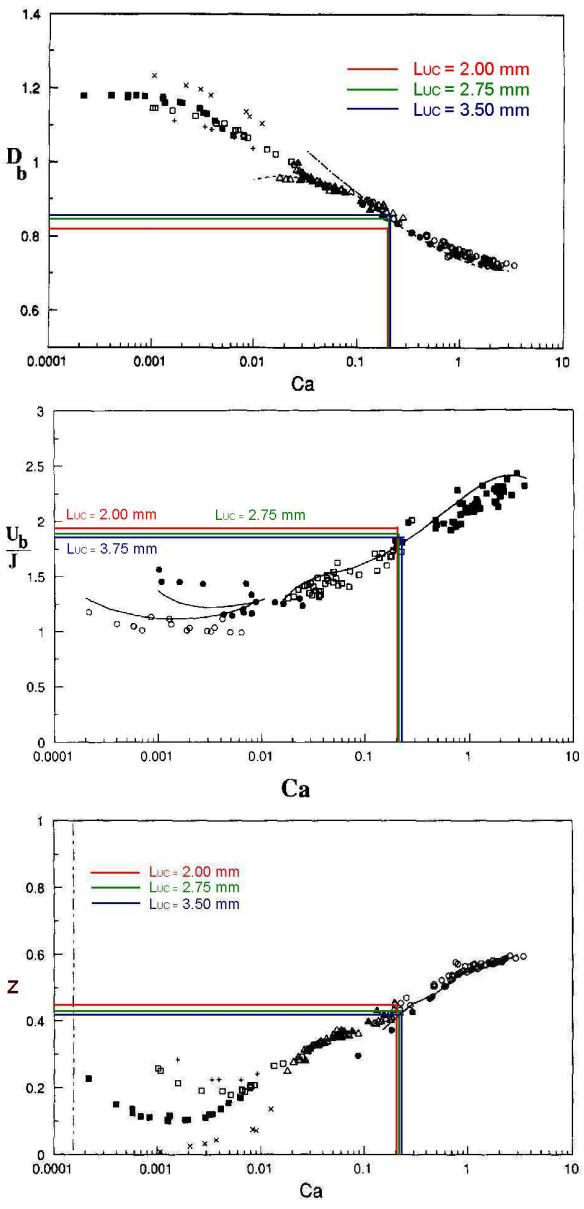

Figure 5: Comparison of d_B/d_h (top), U_B/J (middle) and Z (bottom) over Ca for case A, B, and C with experimental data from Thulasidas et al. (1995).

For the flow hydrodynamics, good agreement with experimental data (Thulasidas et al. 1995) is obtained in terms of non-dimensional bubble diameter, ratio of bubble velocity to total superficial velocity and relative velocity, as displayed in Figure 5. The total superficial velocity is defined as

$$J \equiv \varepsilon U_B + (1-\varepsilon) U_L \tag{21}$$

while the relative velocity is defined as

$$Z \equiv \frac{U_B - J}{U_B} \tag{22}$$

The discrete values of the dimensionless bubble diameter, ratio of bubble velocity to total superficial velocity and relative velocity are listed in Table 4.

In this paper, we will interpret the results for mass transfer mainly in terms of the non-dimensional mean species concentration in the gas phase. This time-dependent quantity is computed as the mean species concentration in the bubble at a certain instant in time divided by the initial concentration in the bubble. While initially its value is unity, it asymptotically approaches a smaller value for long times. As we use periodic boundary conditions not only for the hydrodynamics but also for the species transport equation, this asymptotic value can be computed from a simple species mass balance

$$c_G^0 \, V_G = c_G^{eq} \, V_G + c_L^{eq} \, V_L \,, \tag{23}$$

where V_G and V_L are the volume of the bubble and of the liquid within the unit cell. With the definition of the Henry number, Eq. (13), and that of the gas holdup $\varepsilon \equiv V_G/(V_G + V_L)$ we obtain from Eq. (23) the result:

$$\frac{c_G^{eq}}{c_G^0} = \frac{1}{1 + H\left(1/\varepsilon - 1\right)} \tag{24}$$

Here, simulations of mass transfer are considered for two values of H, namely H = 0.03 and H = 3. For H = 0.03, the normalized mean gas concentration at

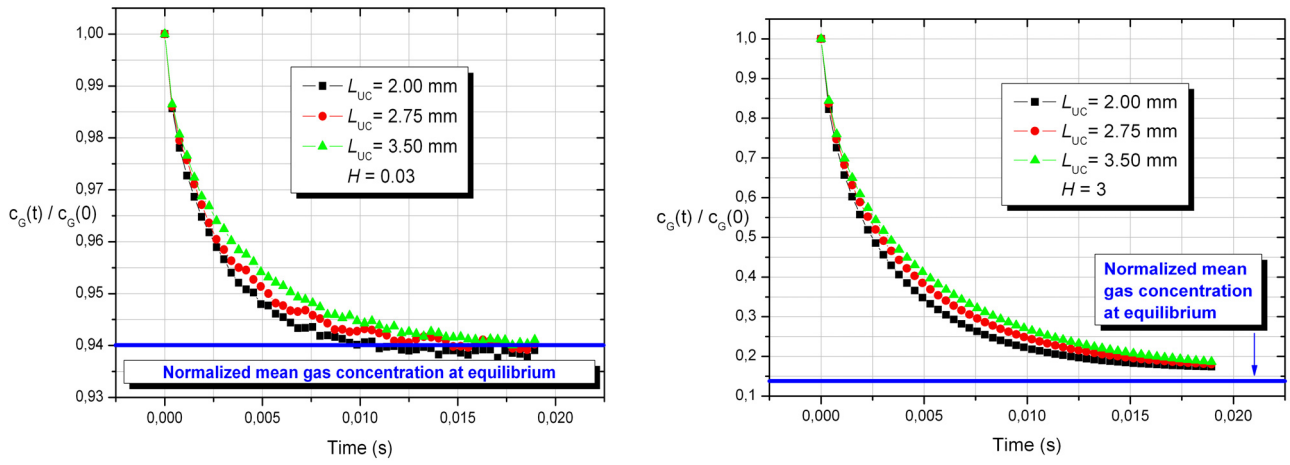

Figure 6: Normalized mean gas concentration for different values of the unit cell length in case of mass transfer without chemical reaction for $H = 0.03$ (left) and $H = 3$ (right).

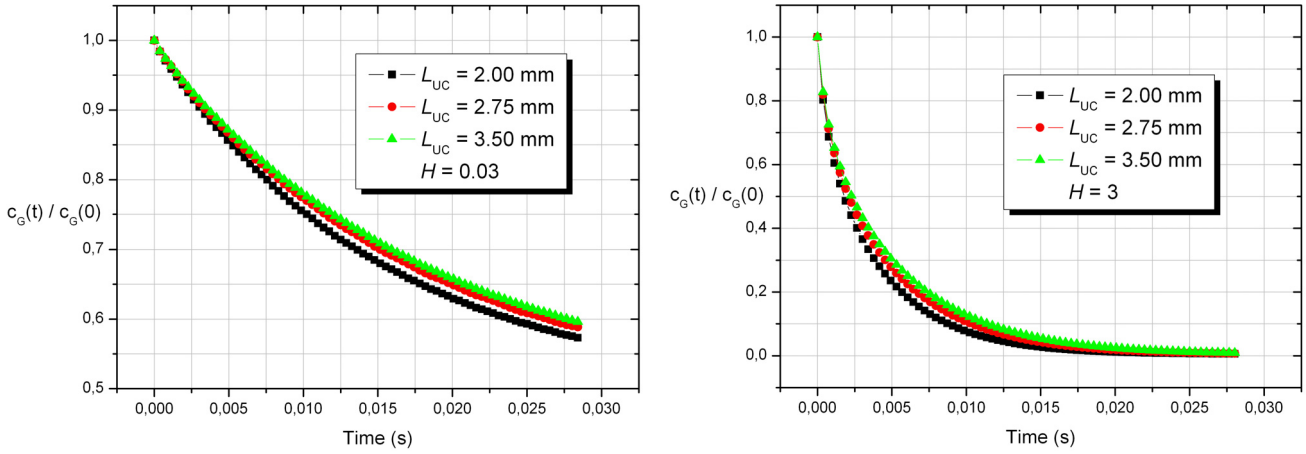

Figure 7: Normalized mean gas concentration for different values of the unit cell length in case of mass transfer with species consumption by a first order homogeneous reaction for $H = 0.03$ (left) and $H = 3$ (right).

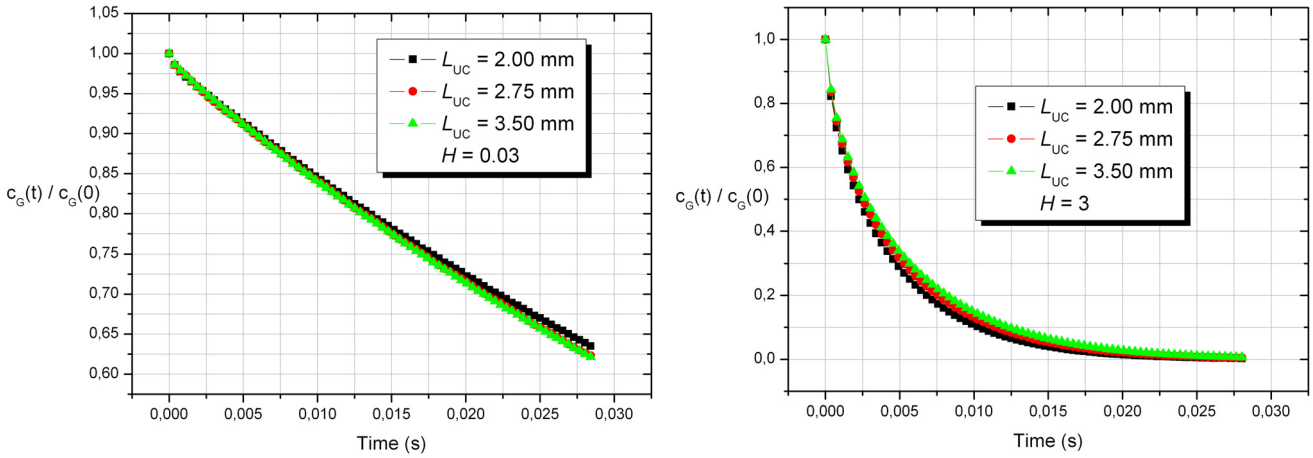

Figure 8: Normalized mean gas concentration for different values of the unit cell length in case of mass transfer with species consumption by a first order heterogeneous reaction for $H = 0.03$ (left) and $H = 3$ (right).

equilibrium is $c_G^{eq}/c_G^0 = 0.94$, shown in Figure 6 (left) by a blue line. As can be seen, the time dependent normalized gas concentration approaches the blue line, denoting the good agreement between the numerical solution and the theoretical value. The gas concentration in cells containing the interface was not considered in the evaluation of the normalized mean gas concentration and therefore the numerical result has a slightly smaller value than the theoretical one. For $H = 3$, the normalized mean gas concentration at equilibrium is $c_G^{eq}/c_G^0 = 0.14$, a value slightly smaller than the numerical data in Figure 6 (right), suggesting that the equilibrium state has not been reached within the actual simulation time.

The results presented in Figure 6 show that short unit cell systems reach the equilibrium state faster than longer unit cell configurations. The same conclusion is reported also by van Baten & Krishna (2004) for mass transfer in Taylor flow operated in circular channels. It should be mentioned that in their numerical study the liquid film between the bubble lateral side and the walls is not saturated.

Longer unit cell configurations exhibit a larger contact area between the bubble lateral sides and the channel walls than short unit cell systems. The liquid film developed in this contact area provides a buffer zone in which mass is rapidly accumulating due to short diffusion lengths and large exposure time. The liquid film becomes very rapidly saturated, decreasing the efficiency of the mass transfer. The occurrence of the saturation can be verified two-fold. The first way is to determine the time of exposure of a mass-less particle flowing within the liquid film, while the second way is to examine the concentration field within the liquid film. We have computed the time of exposure as the ratio between the liquid film length and the liquid velocity in the film, considered in the bubble frame of reference, as displayed in Figure 4. The values obtained agree well with the formulation of the exposure time proposed by Vandu et al. (2005), see Table 5. Based on the exposure times we have calculated the Fourier number as:

$$Fo \equiv \frac{D_L\, t_{exp}}{L_{LF}^2} \tag{25}$$

The exposure time is denoted as short if $Fo < 1$ and as long for $Fo > 1$ (Toor & Marchello, 1958). For long exposure times saturation occurs in the film leading to inefficient local mass transfer.

Table 5: Time of exposure and Fourier number.

Case	A	B	C
L_{LF} (mm)	0.42	0.80	1.18
U_{LF} (m s^{-1})	0.066	0.082	0.095
t_{exp} (ms) – this study	6.36	9.77	12.71
t_{exp} (ms) – Vandu et al. (2005)	6.85	9.42	11.9
Fo (-)	12.22	25.65	39.42

Based on the formulation of the normalized gas concentration at equilibrium, Eq. (24), the value of the concentration at equilibrium in the liquid phase is obtained as

$$\frac{c_L^{eq}}{c_G^0} = H\frac{c_G^{eq}}{c_G^0} = \frac{H}{1 + H\left(1/\varepsilon - 1\right)} \tag{26}$$

For $H = 0.03$, the non-dimensional equilibrium concentration in the liquid is 0.0282, while for $H = 3$ it is 0.423. Figure 9 shows that the concentration in the liquid film is larger than the equilibrium concentration in the liquid.

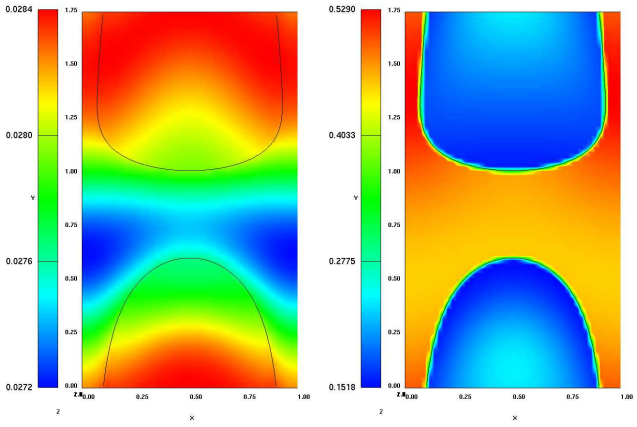

Figure 9: Concentration field in vertical mid-plane for case C at $t \approx$ 0.02 s. The left picture is for $H = 0.03$ and the concentration field c_m is shown, while the right picture is for $H = 3$ and c_L/c_{ref} and c_G/c_{ref} are shown in the liquid and the bubble, respectively.

We have considered the driving force for mass transfer to be constituted by the mean phase concentrations. In this way one can avoid the employment of the bulk concentration and of the concentration at interface, since these are difficult to be defined in small non-circular confined systems. Therefore, the time dependent mass transfer coefficient can be derived to obtain the following expression (Onea 2006):

$$k_L = \frac{V_{uc}}{A_i}\frac{\varepsilon}{\Delta t}\ln\left(\frac{c_G\left(t-\Delta t\right)/H - c_L\left(t-\Delta t\right)}{c_G\left(t\right)/H - c_L\left(t\right)}\right) \tag{27}$$

The mass transfer coefficient k_L for cases A – C is displayed in Figure 10. It can be observed in relation (27) that the mass transfer coefficient is inversely proportional to the interfacial area concentration. As displayed in Table 4, the interfacial area concentration A_i/V_{uc} is proportional to the unit cell length indicating that short unit cells are more efficient for mass transfer than long unit cells.

For mass transfer with first order chemical reaction, the reaction constant was set to $k_{hmg} = 1500$ s^{-1} for the homogeneous reaction, while for the heterogeneous reaction it was set to $k_{htg} = 50$ m s^{-1}. For all cases in the present study in which the species is consumed by a homogeneous chemical reaction it was considered that the reaction occurs only if the solute exceeds 1.5% from the initial gas concentration.

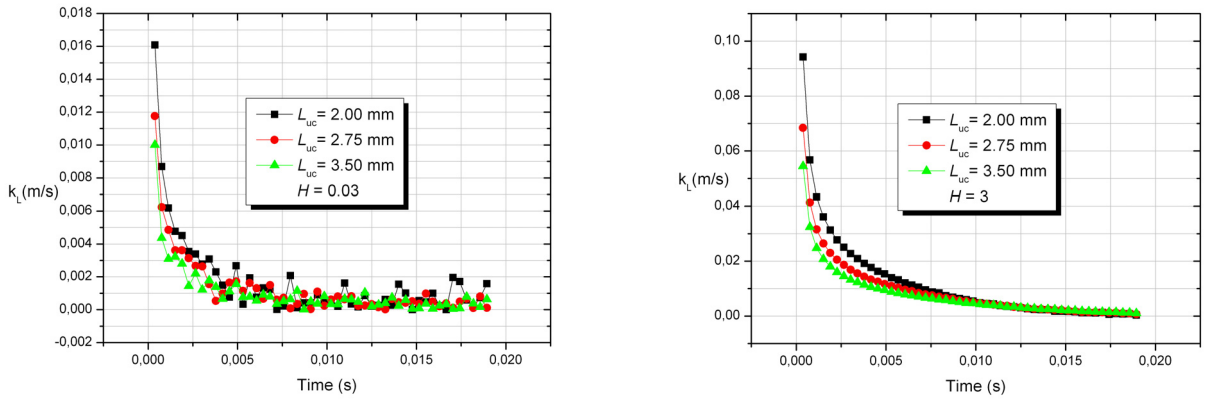

Figure 10: Mass transfer coefficient determined with formula (27) for $H = 0.03$ (left) and $H = 3$ (right).

In case of mass transfer with species consumption by a first order homogeneous chemical reaction, small unit cells systems transfer more solute per time into the continuous phase than long unit cell systems. This is valid for both values of the Henry number, see Figure 7. Since more mass is transferred per time in the liquid phase by small unit cell systems, the amount of mass available for reaction is also larger. In the present case, the value of the Damköhler number

$$Da_{\mathrm{hmg}} = \frac{k_{\mathrm{hmg}} d_{\mathrm{h}}^2}{D_{\mathrm{L}}} = 96.4 \qquad (28)$$

is large suggesting that the chemical reaction has a fast character. The largest part of mass transfer occurs at the bottom of the bubble as displayed in Figure 11, since the bubble exhibits the largest local interfacial area at the bottom. It can be observed in Figure 11 that the concentration in the liquid phase does not exceed the minimum dimensionless concentration $c_{\mathrm{min}}/c_{\mathrm{ref}} = 0.015$ at which the reaction occurs and that the concentration in the liquid is uniform. Both aspects are attributable to the fast character of the chemical reaction.

In case of mass transfer with species consumption by a first order heterogeneous chemical reaction the results are displayed in Figure 8 in terms of the normalized mean gas concentration. The results obtained for small Henry number, i.e. $H = 0.03$, suggest that the long unit cell configurations tend to be slightly more efficient, since they benefit from a longer liquid film, where a significant part of mass is consumed. In case of large Henry number, i.e. $H = 3$, the small unit cell systems tend to transfer more solute, suggesting that the contribution of the liquid slug is also important when the mass flux is large.

The concentration field in vertical mid-plane for case C is displayed in Figure 12. For small unit cells (not shown) the mass consumption at the walls is almost uniform in axial direction. For the long unit cell of case C, the bottom part of the bubble, as well as the liquid slug, contribute only slightly to the overall mass transfer, since the concentration gradient is rapidly decreasing within these regions. The value of the Damköhler number for the heterogeneous reaction is large, signifying that the reaction is fast:

$$Da_{\mathrm{htg}} = \frac{k_{\mathrm{htg}} d_{\mathrm{h}}}{D_{\mathrm{L}}} = 1606.68 \qquad (29)$$

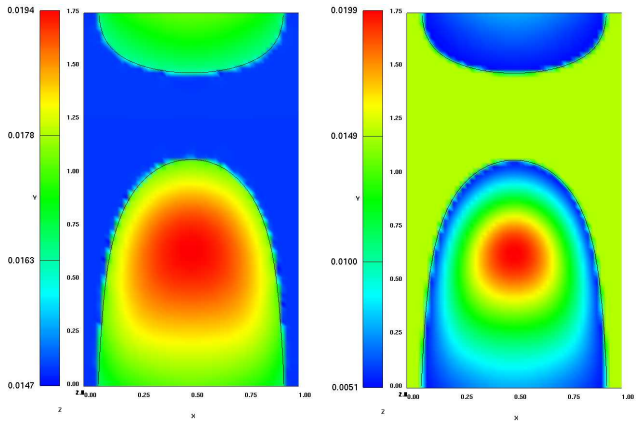

Figure 11: Concentration field in vertical mid-plane for case C in case of mass transfer with homogeneous reaction at $t \approx$ 0.03 s. The left picture is for $H = 0.03$ and the concentration field c_{m} is shown, while the right picture is for $H = 3$ and $c_{\mathrm{L}}/c_{\mathrm{ref}}$ and $c_{\mathrm{G}}/c_{\mathrm{ref}}$ are shown in the liquid and the bubble, respectively.

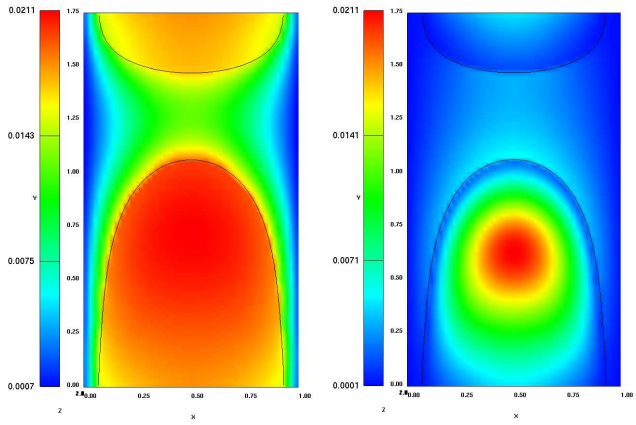

Figure 12: Concentration field in vertical mid-plane for case C in case of mass transfer with heterogeneous reaction at $t \approx$ 0.03 s. The left picture is for $H = 0.03$ and the concentration field c_{m} is shown, while the right picture is for $H = 3$ and $c_{\mathrm{L}}/c_{\mathrm{ref}}$ and $c_{\mathrm{G}}/c_{\mathrm{ref}}$ are shown in the liquid and the bubble, respectively.

3.3 Influence of the liquid slug length

In order to investigate the influence of the liquid slug length on mass transfer two cases have been considered, as displayed in Table 6. The coordinate system, physical parameters of the fluids and the mass transfer parameters are considered as in the previous section (see Table 3). The pressure drop was adjusted so that a similar bubble velocity could be obtained. While only the Henry number $H = 0.03$ is considered, two values for the constant of the homogeneous chemical reaction have been employed, namely $k_{hmg} = 15\ s^{-1}$ for a slow reaction and $k_{hmg} = 1500\ s^{-1}$ for a fast reaction. For the heterogeneous reaction, the constant of the slow reaction was set to $k_{htg} = 0.005\ m\ s^{-1}$ for a slow reaction and $k_{htg} = 50\ m\ s^{-1}$ for a fast reaction. The time step width used is again $\Delta t / t_{ref} = 2.5 \times 10^{-5}$.

Table 6: Parameters for the study of the influence of the liquid slug length on mass transfer.

Case	D	E
$L_x = L_z = L_{ref}$ (mm)	2.0	2.0
L_y (mm)	2.75	3.33
Grid	48×66×48	48×80×48
ε (-)	33.0	24.7
Eu_{ref} - Fr_{ref} (-)	27.03	35.82
L_B (mm)	2.27	2.16
L_{LS} (mm)	0.48	1.173
U_B (m s^{-1})	0.099	0.100
U_L (m s^{-1})	0.035	0.042
A_i/V_{uc} (m^{-1})	1476.45	1369.35

As can be seen in Table 6, the bubbles have almost the same length, meaning that the contribution of the liquid film to mass transfer is similar. However, increasing the length of the liquid slug while keeping the bubble length about constant corresponds to a decrease of the gas hold-up, see Table 6. Therefore, the normalized mean gas concentration at equilibrium is smaller for case E than for case D, see Figure 13. This means that in case E more species is transferred from the gas into the liquid phase simply because more liquid is available as solvent than in case D. However, to estimate which system is more efficient for mass transfer, one should not consider the normalized mean gas concentration since its asymptotic value is different for both cases. In order to estimate which system transfers globally more mass, we have considered the concentration in the liquid divided by the unit cell length, as displayed in Figure 14. The evaluation of the volumetric mass transfer coefficient with relation (27) reveals that shorter liquid slugs are more efficient for mass transfer than long liquid slugs. This result is in good qualitative agreement with the experimental results of Berčič & Pintar (1997) for gas-to-liquid mass transfer in Taylor flow in circular capillaries, where the importance of the liquid slug length is discussed and where the volumetric mass transfer coefficient $k_L A_i/V$ is found to be proportional to the product $[(1 - \varepsilon)\ L_{uc}]^{-0.57}$. Also Kreutzer et al. (2001) find from axisymmetric CFD computations that the mass transfer from the liquid slug to the wall is enhanced for short liquid slugs.

In case of mass transfer with species consumption in the continuous phase by homogeneous chemical reaction, for both cases of slow ($Da_{hmg} = 0.964$) and fast reaction ($Da_{hmg} = 0.964$) more species per unit cell length is transferred in the liquid for the system having short liquid slug, as presented in Figure 15. The amount of mass transferred into the liquid phase has been calculated as $c_L(t) = (c_G(0) - c_G(t))\ \varepsilon / (1 - \varepsilon)$. As the chemical reaction becomes faster, the efficiency of the shorter liquid slug decreases. Therefore, the length of the liquid slug plays a role if the chemical reaction has a slow character. It can be concluded that a critical constant of the chemical reaction exists. If this critical value is not exceeded, the configurations having short liquid slugs will benefit from the increased amount of mass transferred per unit length, otherwise no significant influence on mass transfer will be observed.

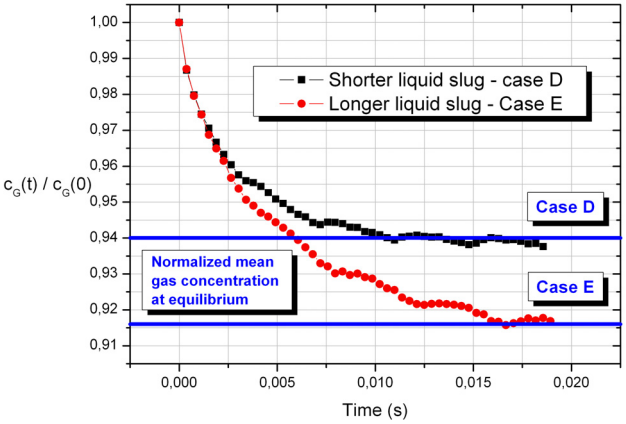

Figure 13: Comparison of normalized mean gas concentration for short and long liquid slug lengths.

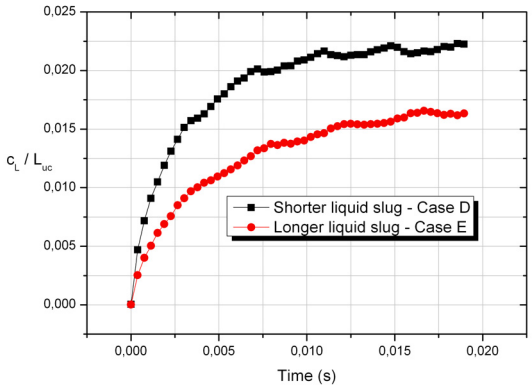

Figure 14: Comparison of ratio of dimensionless mean liquid concentration c_L/c_{ref} to dimensionless unit cell length L_{uc}/L_{ref} for short and long liquid slugs.

In case of mass transfer with species consumption at the walls by a first order heterogeneous chemical reaction, the short liquid slug configuration is more efficient than the long one per unit length if the chemical reaction is slow. The amount of species transferred in the liquid per unit cell length, which was determined similar to the previous case, is displayed in Figure 16. In accordance with the previous case it can be concluded that as the reaction becomes faster the efficiency of the short liquid slug decreases and that a critical constant of the chemical reaction exists. The Damköhler number for the slow reaction is $Da_{htg} = 0.1606$, while for the fast reaction it is 10^4 times larger. As a consequence of the permanent and fast mass consumption no species recirculation in the bubble or in the liquid is observed for both cases of mass transfer with chemical reaction.

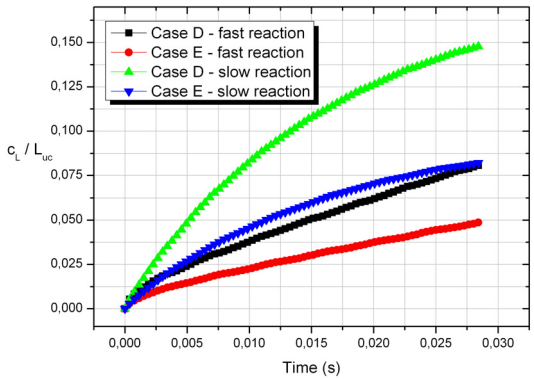

Figure 15: Comparison of ratio of dimensionless mean liquid concentration c_L/c_{ref} to dimensionless unit cell length L_{uc}/L_{ref} for short and long liquid slugs in case of mass transfer with slow and fast homogeneous chemical reaction in the liquid phase.

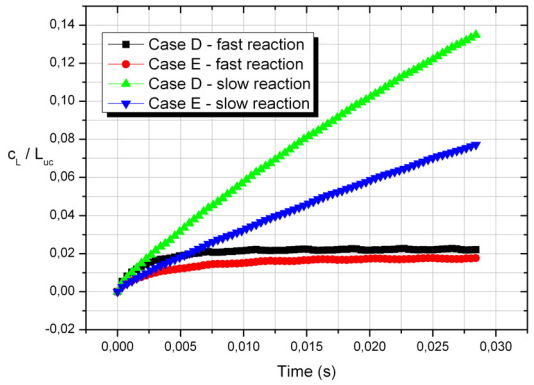

Figure 16: Comparison of ratio of dimensionless mean liquid concentration c_L/c_{ref} to dimensionless unit cell length L_{uc}/L_{ref} for short and long liquid slugs in case of mass transfer with slow and fast heterogeneous chemical reaction.

3.4 Influence of the channel aspect ratio

To investigate the influence of the shape of the channel cross section, three unit cell configurations having an aspect ratio ranging from 1 to 1.6 have been considered. In order to ensure the same basis for the hydrodynamics and mass transfer, all three systems share the same hydraulic diameter of d_h = 2 mm and the same gas content of 33%. The pressure drop was adjusted to obtain for all cases the same value for the product $Re_B Sc_L = d_h U_B / D_L$. The physical properties of the fluids are the same as in Table 3, while the parameters of the simulations are given in Table 7. Only the Henry number $H = 0.03$ is considered.

Figure 17 shows cross sections through the bubble at representative axial positions in the channel. As can be seen, the bubble in the square channel has a circular cross-section while for the bubbles in the rectangular channels the shape is ellipsoidal. Due to this strong deformation of the bubble the volumetric interfacial area concentration A_i/V_{uc} is significantly increasing with increasing aspect ratio, see Table 7.

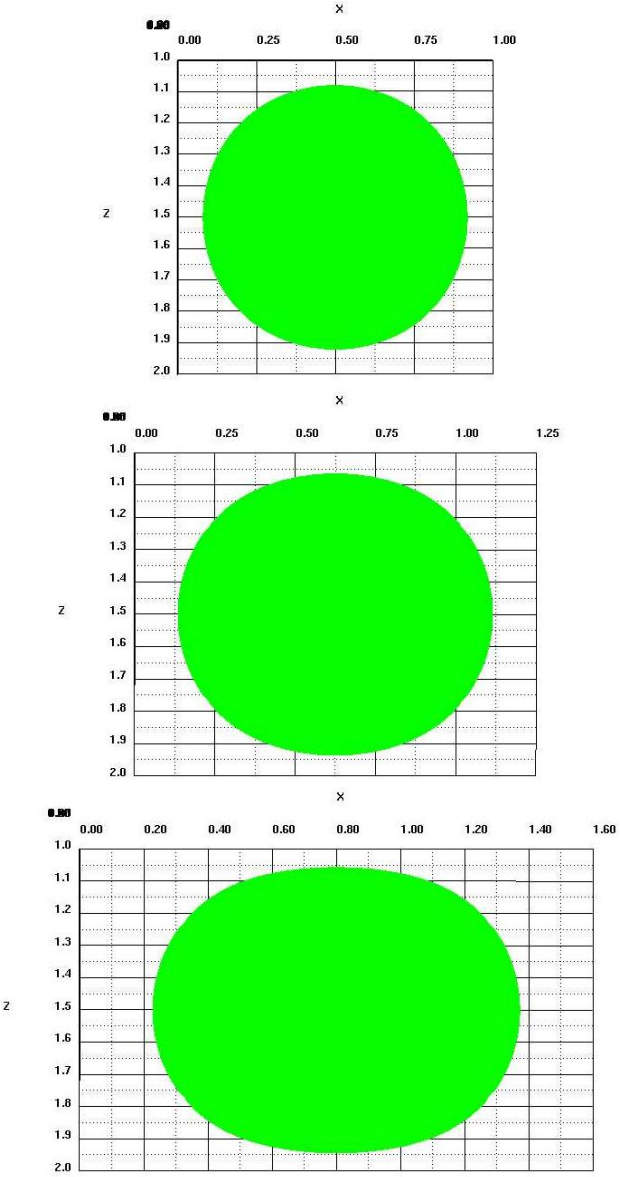

Figure 17: Bubble shape in *x-z* cross section at representative axial positions for cases F, G and H. Note that *x* and *y* are made dimensionless by L_{ref} which differs for each case.

Table 7: Parameters for the study of the influence of the channel aspect ratio on mass transfer.

Case	F	G	H
L_x (mm)	2.0	2.25	2.6
L_y (mm)	2.5	2.475	2.4375
$L_z = L_{ref}$ (mm)	2.0	1.8	1.625
Aspect ratio L_x/L_z (-)	1	1.25	1.6
Grid	48×60×48	60×66×48	64×60×40
Eu_{ref} - Fr_{ref} (-)	27.03	24.00	21.24
U_B (m s^{-1})	0.0956	0.0956	0.0956
U_L (m s^{-1})	0.034	0.033	0.03
L_B (mm)	2.1	2.115	2.215
L_{LS} (mm)	0.4	0.36	0.22
A_i/V_{uc} (m^{-1})	1340	1883.3	2633.8
Da_{hmg} / ($Re_B Sc_L$) (-)	87.82	90.12	98.81
Da_{htg} / ($Re_B Sc_L$) (-)	1463.7	1501.95	1646.9
Δt / t_{ref} (-)	2.5×10^{-5}	2.0×10^{-5}	2.5×10^{-5}

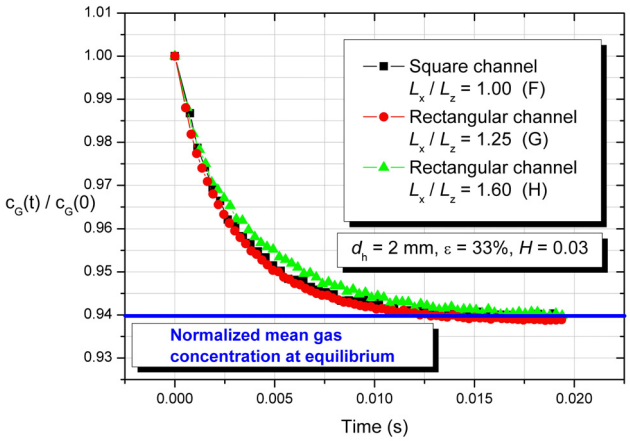

Figure 18: Influence of channel aspect ratio on mass transfer.

The theoretical and the numerical results for the normalized mean gas concentration for pure mass transfer are displayed in Figure 18. The blue line is again determined with expression (24). No significant difference between case F and G can be observed. Despite this fact it can be concluded that the small aspect ratio channels approach equilibrium slightly faster than the larger aspect ratio channel of case H. The reason for this may be that the large aspect ratio channel exhibits a thinner and very fast saturated liquid film along the depth of the channels than small aspect ratio channels though the interfacial area concentration for case H is much higher than for case F and G.

In case of mass transfer with species consumption in the continuous phase by a first order homogeneous chemical reaction, the results presented in Figure 19 show that more mass is transferred in the liquid for the channels that have an aspect ratio larger than unity. The channel with aspect ratio 1.25 is the most efficient one, whereas a further increase of the aspect ratio to 1.6 for case H results in slightly slower mass transfer. However, the mass transfer for case H is still faster than for case F with the square channel. For mass transfer with species consumption by a first order heterogeneous chemical reaction at the channel walls the tendency can be observed in Figure 20 that large aspect ratio channels are more efficient.

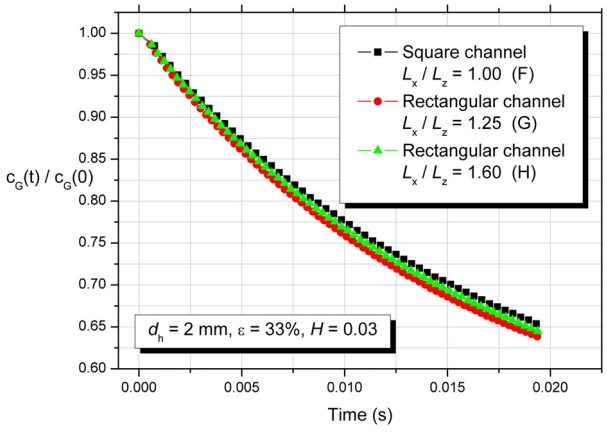

Figure 19: Influence of channel aspect ratio on mass transfer with first order homogeneous chemical reaction.

Both, for the homogeneous and the heterogeneous chemical reaction the ratio Da / ($Re_B Sc_L$) is larger than 10 suggesting that the chemical reaction considered is fast (Gartsman et al., 1979). The constant of the homogeneous reaction is k_{hmg} = 1500 s^{-1}, while for the heterogeneous chemical reaction at the walls it is k_{htg} = 50 m s^{-1}. For both cases the enhanced efficiency of the large aspect ratio channels may be attributable to the fast occurrence of the chemical reaction within the liquid film.

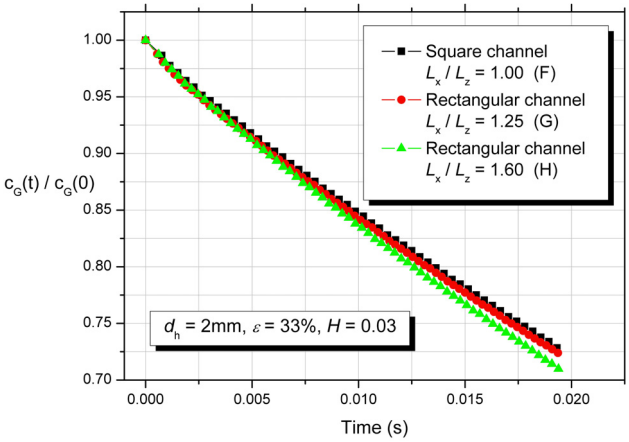

Figure 20: Influence of channel aspect ratio on mass transfer with first order heterogeneous chemical reaction.

4. Conclusions

Based on the volume-of-fluid method for interface tracking, a computer code has been developed for numerical simulation of mass transfer with optional species consumption by a first order chemical reaction in the continuous phase or at the channel walls. Employing Henry's law, the concentration field is allowed to be discontinuous at interface. The numerical method has been validated by comparison to one and two-dimensional mass transfer problems with known analytical solution.

The code developed has been used to investigate the low Schmidt number mass transfer of an artificial species from the gas into the liquid phase in bubble train flow within a mini-channel. A series of simulations has been performed to investigate the influences of the unit cell length, liquid slug length and of the channel aspect ratio on the efficiency of mass transfer. The study of the influence of the unit cell length for square channels revealed that short unit cells are more efficient for mass transfer with and without chemical reaction.

As concerns the influence of the length of the liquid slug, for all cases of mass transfer with and without chemical reaction, the systems with short liquid slugs transfer more solute per unit length. In case of mass transfer only the equilibrium concentrations are reached faster in configurations with a shorter liquid slug. In case of mass transfer with a homogeneous or heterogeneous chemical reaction the influence of the liquid slug length decreases if the chemical reaction becomes faster.

The study of the influence of the aspect ratio of the rectangular channel revealed that square channels or channels with an aspect ratio close to one are best suited for mass transfer without chemical reaction, while channels with an aspect ratio different from unity are more efficient when a homogeneous or heterogeneous chemical reaction is considered.

While in the present paper the mass transfer of an artificial species at a Schmidt number of order one has been considered, in practical applications usually much larger Schmidt numbers are encountered. The present numerical method is not restricted with respect to Schmidt number, however, an adequate resolution of the thin concentration boundary layer is essential and much finer grids are required than have been used here. Our next goal is, therefore, to use the code to investigate interfacial mass transfer in bubble train flow at higher values of the Schmidt number.

References

Apelblat, A. – Mass transfer with a chemical reaction of the first order: analytical solutions. Chem. Eng. J. 19, 19 – 37, 1980

Berčič, G. & Pintar, A – The role of gas bubbles and liquid slugs lengths on mass transport in the Taylor flow through capillaries, Chem. Eng. Sci. 52, 3709 – 3719, 1997

Bothe, D., Koebe, M., Wielage, K., Warnecke, H.J. – VOF-Simulations of mass transfer from single bubbles and bubble chains rising in aqueous solutions. Proc. 4th ASME-JSME Joint Fluids Engineering Conference, Honolulu, Hawaii, USA, July 6-11, 2003

Bothe, D., Koebe, M., Wielage, K., Prüss, J., Warnecke, H.J. – Direct numerical simulation of mass transfer between rising gas bubbles and water. In M. Sommerfeld (Ed.): Bubbly flows. Analysis, modelling and calculation., Springer Verlag, 159 – 174, 2004

Crank, J. – The mathematics of diffusion, Oxford – Claredon Press 2nd edition, 1994

Davidson, M.R., Rudman, M. – Volume-of-fluid calculation of heat or mass transfer across deforming interfaces in two-fluid flow, Numerical Heat Transfer B, 41, 291 – 308, 2002

Gartsman, A.N., Cherkashin, V.V. and Rassadnikova, N. N. – Diffusion flux through a spherical gas-liquid interface in the presence of a chemical reaction in the liquid phase, Int. Chem. Eng. 19, 356 – 360, 1979

Ghidersa, B., Wörner, M. and Cacuci, D.G. – Exploring the flow of immiscible fluids in a square vertical mini-channel by direct numerical simulation, Chem. Eng. J. 101, 285–294, 2004

Hasegawa, Y. & Kasagi, N. – Effects of interfacial velocity boundary condition on turbulent mass transfer at high Schmidt numbers. In K. Hanjalic, Y. Nagano, S. Jakirlic (Eds.): Turbulence, Heat and Mass Transfer 5, Begell House, pp. 1–11, 2006

Irandoust, S. & Andersson, B. – Mass transfer and liquid phase reactions in a segmented two-phase flow monolithic catalyst reactor, Chem. Eng. Sci. 43, 1983 – 1988, 1988

Irandoust, S. & Andersson, B. – Simulation of flow and mass transfer in Taylor flow through a capillary, Comput. Chem. Eng. 13, 519 – 526, 1989

Koynov, A., Khinast, J.G. & Trygvasson, G. – Mass transfer and chemical reactions in bubble swarms with dynamic interfaces, AIChE J. 51, 2786 – 2800, 2005

Kreutzer, M.T., Du, P., Heiszwolf, J.J., Kapteijn, F. & Moulijn, J.A. – Mass transfer characteristics of three-phase monolith reactors, Chem. Eng. Sci. 56, 6015 – 6023, 2001

Ohta, M. & Suzuki, M. – Numerical analysis of mass transfer from a free motion drop in a solvent extraction process, Solvent Extraction Res. Dev. 3, 138 – 149, 1996

Onea, A. – Numerical simulation of mass transfer with and without first order chemical reaction in two-fluid flows, PhD Thesis, University of Karlsruhe, 2006 (http: //www.ubka.uni-karlsruhe.de/cgi-bin/psview?document=/2007/maschinenbau/7&search=/2007/maschinenbau/7)

Paschedag, A.R., Piarah, W.H., & Kraume, M. – Treatment of limits for mass transfer at single droplets – validation of numerical results, Chem. Eng. Technol. 25, 953 – 956, 2002

Paschedag, A.R., Piarah, W.H., & Kraume, M. – Sensitivity study for the mass transfer at a single droplet, Int. J. Heat Mass Transfer 48, 3402 – 3410, 2005

Patankar, S. V. – Numerical heat transfer and fluid flow, Taylor and Francis, 1980

Petera, J. & Weatherley, L.R. – Modelling of mass transfer from falling droplets, Chem. Eng. Sc. 56, 4929 – 4947, 2001

Sabisch, W., Wörner, M., Grötzbach, G. & Cacuci D.G. – 3D Volume-of-fluid simulation of a wobbling bubble in a gas-liquid system of low Morton number, Proc. 4th Int. Conf. Multiphase Flow, May 27-June 1, 2001, New Orleans, LA, USA

Thulasidas, T.C., Abraham, A.C., Cerro, R.L. – Bubble-train flow in capillaries of circular and square cross-section, Chem. Eng. Sci. 50, 183 – 199, 1995

Toor, H. L. & Marchello, J.M. – Film-penetration model for mass and heat transfer, AIChE J. 4, 97 – 101, 1958

van Baten, J.M. & Krishna, R. – CFD simulations of mass transfer from Taylor bubbles rising in circular capillaries, Chem. Eng. Sci. 59, 2535 – 2545, 2004

Vandu, C.O., Liu, H. and Krishna, R. – Mass transfer from Taylor bubbles rising in single capillaries, Chem. Eng. Sci. 60, 6430 – 6437, 2005

Wörner, M., Ghidersa, B., Shahab, A.F. – Numerical study of bubble train flow in a square vertical mini-channel: influence of length of the flow unit cell, 5th Int. Conf. Multiphase Flow, Yokohama, Japan, Paper no. 154, 2004

Wörner, M., Ghidersa, B., Onea, A. – A model for the residence time distribution of bubble-train flow in a square mini-channel based on direct numerical simulation results, Int. J. Heat Fluid Flow 28, 83 – 94, 2007

Yang, C. & Mao, Z.-S. – Numerical simulation of interphase mass transfer with the level set method, Chem. Eng. Sc. 60, 2643 – 2660, 2005